Charge and Discharge Characterization of Lithium-ion Electrode Materials Through Coin Cell Testing

An Undergraduate Honors Thesis

Department of Mechanical Engineering

The Ohio State University

Jiahui Liu

Spring, 2015

Dr. Marcello Canova, Advisor

Abstract

Lithium-ion batteries play a fundamental role in the development and commercial success of electric vehicles, due to their higher charge and discharge efficiency, and their high energy density. On the other hand, significant research challenges are still present, for instance understanding and mitigating the degradation processes that lead to capacity and power fade in batteries, as well as prototyping and characterizing new materials for improving the energy density, safety, and reduce costs.

In this scenario, coin cell testing is a very important experimental technique to analyze the performance of Lithium-ion batteries, and collect data to develop and verify behavioral models that can describe the charging and discharging dynamics and the voltage response of the battery in presence of variable input current.

The proposed research project focuses on studying the process of analyzing the charging/discharging performance of Li-ion cell electrode materials through coin cell fabrication and half-cell testing. By analyzing the experimental data, important information can be found on the charging and discharging performance and efficiency of the cell. In addition, the dynamics of the lithium transport process can be assessed, as well as its dependence on usage and environmental factors such as C-rate, State of Charge (SOC) and temperature. This study will provide quantitative information on the physical and chemical properties of electrode materials, and improve our understanding on how such materials can improve the energy density, safety, and reduce costs of Lithium-ion batteries.

Acknowledgements

I would like to thank Dr. Marcello Canova for being my advisor on this project. He introduced me to the project and has helped to guide me towards completion of the project, even with the multiple obstacles we have faced. With his extremely busy schedule, he still chose to meet with me on a regular basis and provided important feedback and direction in order to guide me towards successful completion of this project.

I would also like to thank Alex Bartlett for his guidance in the lab and feedback on this project. He helped with experimental design, gave valuable knowledge on coin cell fabrication and testing.

In addition, I would like to thank the Ohio State Center for Automotive Research for allowing me to do my research at its facilities.

Table of Contents

List of Figures

List of Tables

Chapter 1: Introduction

1.1. Motivation for Li-ion battery research

The large of number of automobiles currently in use around the world have caused and are still causing serious problems such as air quality, global warming and depletion of primary energy resources. Because of the rapidly increasing fuel costs and stringent emissions standards, it is necessary to develop a safe, clean and highly efficient transportation [1]. To meet the revolutionary challenge, major automotive manufacturers release the hybrid and electric vehicles onto the market. Toyota launched Prius in 1997 [2], still today, it is first electrified vehicle on the market. And Tesla Model S was named “Motor Trend’s Car of the Year” introduced in 2012 [3].

Currently, Lithium-ion batteries are the solution of choice for hybrid and electric vehicles due to the high energy density and long life cycle [4]. Specific power is the maximum power available per unit mass, and determines battery weight for a given power target. Specific energy is the nominal battery energy per unit mass which determines battery weight to achieve an electric range. As seen in Figure 1, Li-ion Batteries cover a wider range of specific energy and specific power while compared to other battery types. In a hybrid electric vehicle, a battery pack is used to provide propulsion along with the internal combustion engine, while in an electric vehicle, the battery pack provides all the power. The battery pack is charged and discharged repeatedly during vehicle operation.

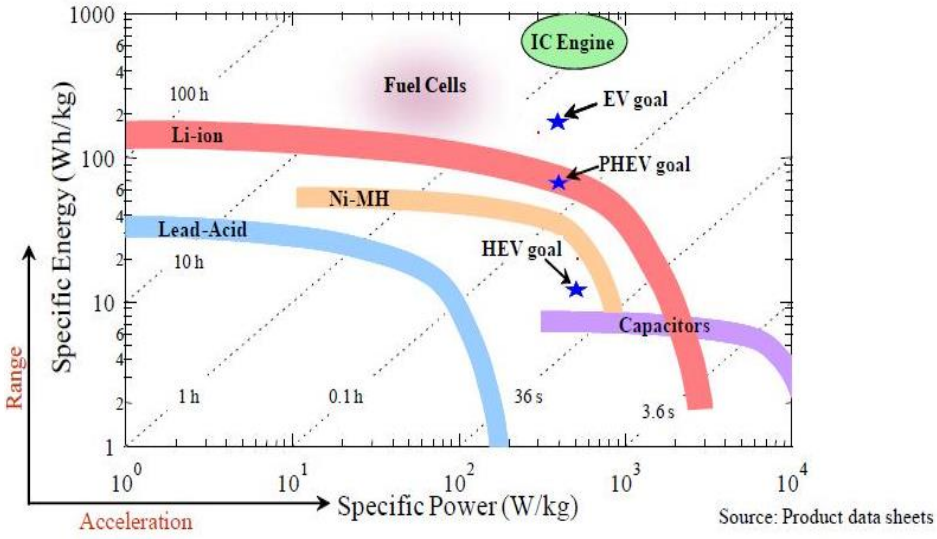

Figure 1 The Ragone Plot for Various energy storage devices [6]

However, there are some limits in the current battery technologies that pose constrains to the performance of electric vehicles, such as the driving range, as well as to the high purchase and warranty costs. It has been estimated that a reduction of 30% in the costs and an increase of energy density of two times over the current state of the art will be needed to facilitate a larger penetration of electric vehicle in the market [5]. In order to satisfy the above requirements, it is critical to find ways to improve the performance of Lithium-ion batteries and to reduce their production costs, for instance through the development of new electrode materials.

This project will focus on characterizing the charge/discharge characterization of Lithium-ion battery materials to understand how their performance correlates with usage conditions and environmental factors. It is expected that this research will provide quantitative information on the physical and chemical properties of electrode materials, and improve our understanding on how such materials can improve the energy density, safety, and reduce costs of Lithium-ion batteries.

1.2. Objective

The purpose of this research is to determine the charge/discharge behavior of electrode materials for Lithium-ion batteries using coin cell testing. Specifically, the proposed research objectives include:

- Fabricate half cells of Lithium Iron Phosphate coin cell using cathode materials harvested from A123 cells to study the charge and discharge behavior.
- Use the instruments at OSU-CAR to test Lithium-ion coin cells prototypes focusing on the formation cycling and capacity assessment.
- Cycle coin cells and measure relevant parameters including capacity, resistance, state of charge and open-circuit voltage, to understand the charge and discharge behavior for each individual cell.
- Analyze the relationship between capacity, resistance and cycle number when charging and discharging.

In this project, coin cell prototypes will be used to perform different tests, including current and voltage cycling, and capacity testing. The experimental data collected in this research will be also used to study the dynamics of the lithium transport process and determine the influence of several usage and environmental factors such as C-rate, State of Charge (SOC) and temperature on the voltage response to a transient input current profile.

Chapter 2: Background

2.1. Definitions

The terminal voltage is the voltage between the battery terminals when a load is applied. The open-circuit voltage (OCV) is the voltage between the battery terminals when there is no load applied.

The internal resistance is an overall resistance within the battery which varies with charge level and temperature, and generally different or charging and discharging. When the internal resistance is increased, the batter efficiency decreases due to more charging energy is converted to heat.

The battery capacity is the amount of electric charge it can store in a specific condition. The capacity is measured by discharging a fully charged battery through a load at a constant current rate. The capacity is calculated by integrating the current in time.

$$\text{capacity} = -\int_{V_{min}}^{V_{max}} I(t)dt \ \ (I > 0 \ means \ discharging) \quad (1)$$

Since the chemical reaction in the battery cells, the capacity of a battery usually depends on the discharge conditions such discharging current rate, temperature and other factors. For example, if the battery is discharged at a relatively high current rate, the capacity would be lower than expected.

Current rate (C-rate) is a measure of the discharge current relative to its capacity. 1C rate indicates to the current at which the battery will fully discharge in one hour. State of charge (SOC) refers to the present available battery capacity as a percentage of nominal capacity.

$$\mathrm{SOC} = SOC_0 - \frac{1}{Ah}\int Idt \qquad (2)$$

In Equation 2, SOC_0 refers to the state of charge at the beginning of testing.

2.2. Basic operating principles of Li-ion Batteries

Li-ion batteries are commanding a greater market share due to their high energy density. Figure 2 shows a schematic diagram of a typical Lithium-ion Cell. A lithium metal oxide ($LiMO_x$), where M stands for metals, and lithiated carbon are the active materials in the positive and negative electrodes. The metals in the positive electrode are transition metals. The active materials are bonded to metal-foil collectors at both ends of the cell and electrically separated by a microporous polymer separator film or gel-polymer. Electrolytes enable lithium ions to move between the positive and negative electrodes. [7]

In this research, electrodes will be extracted from an existing 20Ah lithium-iron phosphate ($LiFePO_4$) prismatic cell from A123, and used to build half-cell the cathode is made of lithium-iron phosphate and the anode is pure lithium metal ($LiFePO_4|Li$). In general, electrochemical reactions occur at the surfaces of electrodes, the interface between electrode and electrolyte accumulates opposite charges to form a double layer, which is like a capacitance [8]. However, a battery cannot operate ideally. When electrons and charged particles traverse the electrolyte, they face a resistance which caused by the conductivity of the electrolyte and the distance between the electrons. This resistive effect causes the internal resistance of battery. Generally, resistance and capacity dominate the response of a battery.

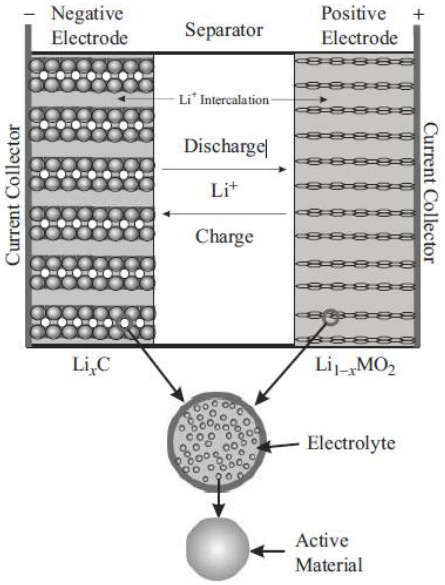

Figure 2 Schematic diagram of a Li-ion cell [7]

In the positive electrode, the active material is oxidized during charge:

$$Li_{1-x}FePO_4 + xLi^+ + xe^- \underset{\text{charge}}{\overset{\text{discharge}}{\rightleftharpoons}} LiFePO_4 \qquad (3)$$

In the negative electrode during charge, the active material is reduced and lithium ions move from the positive electrode and through the separator with the help of electrolyte to the negative electrode:

$$\text{Li} \underset{\text{charge}}{\overset{\text{discharge}}{\rightleftharpoons}} Li^+ + e^- \qquad (4)$$

As Lithium-ion batteries are subjected to multiple cycles, they lose capacity due to the physical and chemical degradation of the positive and negative electrodes, and the electrolyte.

Recent studies have shown that the impedance rise and capacity fade during cycling are primarily due to the positive electrode [9].

2.3. Introduction to charge and discharge testing

The dynamic performance of a battery in charge and discharge is the speed at which current can be put into and taken from storage. The terminal voltage rises and falls during charging and discharging. The charge and discharge dynamics of batteries can be characterized by measurements of voltage under constant charge and discharge current inputs [7]. Figure 3 shows a battery being charged at low, medium and high rates. The high rate discharge case indicates that the voltage drops quickly so that only a part of capacity can be used at high discharge rates.

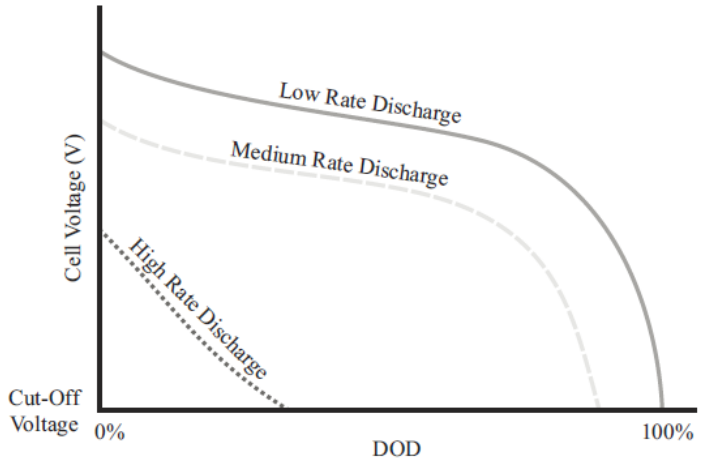

Figure 3 Example voltage curves for different discharge rates [7]

The charge can be controlled by current or voltage. Charging usually consists of periods of constant-current (CC) and/or constant voltage (CV) charging. Figure 4 shows an example CC-CV charging profile. A CC charge is applied initially to bring the voltage up to the CV level. If the CV charge at the beginning, the current will be too high and excessive temperature rise will happen. Once the voltage has been achieved the desired voltage, CV charging begins and the current decreases. If we simply charged a cell until the desired voltage and then cut the current, the cell voltage will

likely drop and eventually stabilize to a value lower than the desired voltage, which indicates that the cell did not fully charged.

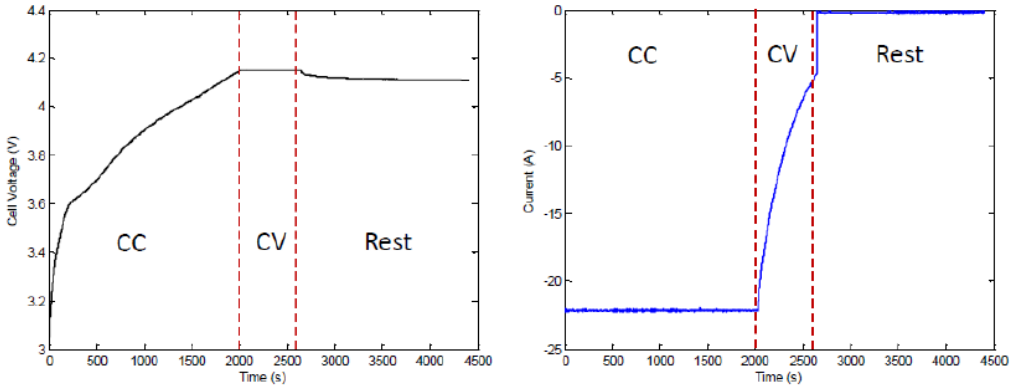

Figure 4 Example of constant-current and constant-voltage charging curve profile

2.4. Overview of formation cycles

Formation cycling is the process that consists of charging and discharging a cell for the first time after it has been assembled. During this process, a cell is cycled multiple times consecutively, using very low current (typically, C/20).

The reason for performing the formation cycles is to gradually build up the film that forms on the surface of the electrodes (called the solid-electrolyte interphase layer - SEI), which allows for a more smooth, stable flow of Li ions and prevents internal shorting. After formation, cells can undergo a suite of initial characterization tests and measurements.

The current profile and test protocols for formation cycling are similar to capacity tests. A capacity test is designed to measure the maximum capacity (or charge) that a cell can supply between two predefined voltage limits. The voltage limits depend on the materials of anodes or cathodes. In case of $LiFePO_4$ cathodes, these limits are typically on the order of 2.5 V lower to 3.6 V upper [10].

Chapter 3: Experimental setup

3.1 Equipment for cell fabrication and characterization

The first stage of this project consists of the fabrication of half-cells using the electrode material harvested from A123 battery packs. Half-cell experiments will allow us to assess the charge and discharge behavior of each electrode. In order to do the fabrication and characterization, the following equipment has been used.

When doing the coin cell fabrication, electrodes and separators are cut by Precision Disc Cutter. This disc cutter, shown in figure 5, is designed for cutting round disc from thin metal sheet. It contains 10 punches which are made from precision ground hardened alloy steel. A hammer is needed to punch the metal through the die.

Figure 5 Precision Disc Cutter (MTI)

An ultrasonic cleaner, shown in figure 6, is a fast and safe cleaning product that utilizes an ultrasonic cleaning process. The cleaner uses ultrasounds (usually from 20–400 kHz) and an appropriate cleaning solvent to clean items. For coin cell fabrication, the ultrasonic cleaner is used to clean the impurities on those elements' surface such as casing, spacer, spring, separator and cathode.

Figure 6 Ultrasonic cleaner (Branson 1510 DTH)

A vacuum oven, shown in figure 7, is used to handle heat-sensitive or oxygen-sensitive substances with unparalleled gentleness when drying. A vacuum or standard atmospheric condition is controlled inside the Vacuum Oven when it is used for process drying. Before the coin cell assembly, all cell components need to be put in the vacuum oven at 75 degree C and leave overnight to dry.

Figure 7 Vacuum oven (VWR Symphony) [11]

The coin cell assembling process is performed in glovebox, shown in figure 8. The glovebox features on automatic regenerable oxygen and moisture single purifier unit so that it can prevent oxygen and moisture pollution of battery material and

sustains an inert Argon atmosphere. The glovebox is designed to develop a clean atmosphere, which can be used to store and operate on air-sensitive materials, such as lithium metals and electrodes. Because the lithium metal is very sensitive to oxygen and water, the coin cell assembly must be done in the glovebox.

Figure 8 Glovebox (MBraun LABstar) [11]

The Compact Hydraulic Crimping machine, shown in figure 9, is then used to seal the coin cell after the assembly to prevent electrolyte leakage. The crimper seals the coin cells by giving a vertical pressure on the coin cells and the pressure periphery. The crimping machine is kept inside the glovebox.

Figure 9 Compact Hydraulic Crimping Machine (MTI MSK-110) [12]

Finally, a Coin Cell Cycler, shown in figure 10, is a testing system for battery and other electrochemical energy storage devices. Each channel of cycler operates independently and runs Galvanostatic Cycling and Cyclic Voltammetry tests on batteries at the same time. In order to ensure the cells are cycled under a specified temperature, cells are put into the environment chamber in which the temperature can be controlled at 25 degrees. Figure 11 shows the specifications of Arbin Coin Cell Cycler.

Figure 10 Coin Cell Cycler (Arbin), with environment chamber (CSZ)

SERIES	2043	2143	2543
Bipolar Linear Circuit Type	Provides zero switching time between charge and discharge		
Voltage Range (max/min)	-10V to 10V		0 to 5V
Accuracy of Voltage Control & Reading 0.02% Full Scale Resolution	±4mV		± 2mV
Current Ranges Provided 0.02% Full Scale Resolution + 0.05% accuracy for 10µA low range	High: 100mA ± 40µA Medium: 1mA ± 0.4µA +Low: 10µA ± 10nA	High: 500mA ± 200µA Medium: 10mA ± 4µA Low: 100µA ± 40nA	High: 5A ± Medium: 100mA ± 40µA Low: 1mA ± 0.4µA
	Medium and Low Current ranges can be customized upon request. Additional delivery time required.		
Minimum V at Maximum Current	-10V @ 100mA	-10V @ 500mA	0V @ 5A
Maximum Continuous Power Output/ Channel	1W	5W	25W
Current Rise Time	100-150µS Time required for current output to get from 10%-90% of requested value		
Current and Voltage Resolution	14 Bit or 0.006%		
Voltage Clamp	Group Voltage Clamp		
Connection for Batteries	Standard 6 ft. cables with alligator clips Arbin can also provide different battery holder options to allow easy engagement of the device to the test station		
Connection to Computer	TCP/IP		
Ventilation Method	Air cooled, front-to-rear airflow		
Room Operating Temperature	10 to 35 degrees C		
Computer Specifications	PC with 22" flat-screen monitor is included, preloaded with our MITS Pro testing software		

Figure 11 Specification of Arbin Coin Cell Cycler

3.2 Coin cell fabrication procedure

3.2.1 Preparing and Cleaning

The materials used to assemble the coin cell included a lithium reference electrode, a cathode, a separator, a spacer, a spring, and coin cell casings. A ring-shaped spring is placed between the negative casing and the spacer in order to ensure adequate pressure is applied to the cell components. The spacer is made from stainless steel. A thin layer of polymer plastic from Celgard Corporation is used as the separator. MTI Corporation provides most materials such as all type coin cases, springs and spacers. The electrolyte is from EMD and contains 1:1 ethylene carbonate and dimethyl carbonate.

There are generally two ways in which working electrode are obtained. One is to harvest the electrode disk from an existing commercial battery that has been disassembled. In this case the electrode may need to be cleaned to remove the impurities on the surface prior to assembly. Another way is to fabricate an electrode from pure materials by mixing together active electrode material powder with a binder.

In this project, electrodes will be taken from an existing 20Ah lithium-iron phosphate (LiFePO4) prismatic cell from A123. However a commercial cell typically contains a double sided electrode. In this case, one of the two sides of each electrode will have to be cleaned to remove the coating. NMP solvent (1-methyl-2-pyrrolidinone) is needed when dissolving the coating. For cleaning, dip a

cotton swab in the NMP and apply it to the electrode coating, making a circular motion to dissolve away the material.

Once the electrode is clean, a 12 mm diameter disk can be cut using the punch. The disk should be soaked in DMC solvent for 10 min in order to remove contaminants from the surface. A thin layer of polymer plastic is used as the separator which should be cut into 18 mm disks using the punch. The separator is 18 mm while the electrode is 12 mm because it is easier to assemble. When assembling, it is hard to make sure all the components are perfectly aligned. If the separator is bigger than the electrode, it is easier to guarantee that the working electrode and counter electrode will be electrically isolated.

Casings, spacer, spring, separator and cathode are placed to be cleaned in a beaker filled with isopropyl alcohol, and then put them into the ultrasonic cleaner for 10 min. These elements need to be cleaned since there may be impurities on their surface. If the cleaning dose not complete before assemble, these impurities may influence coin cell's properties such as capacity and impedance. The counter electrode (Li metal) does not need to be cleaned because lithium is highly reactive and reacts with water and oxygen, so these materials should be kept inside the glovebox at all times.

After the cell components cleaning, one placed in the vacuum oven at 75 degree C and left overnight to dry. The vacuum environment inside lower the boiling temperature of water and facilitates evaporation, in order to avoid damaging the materials from the presence of water.

3.2.2 Assembly

The materials are then transferred to the glovebox after drying. The structure of the coin cell can be seen in Figure 11.

Figure 12 Components of coin cell [13]

When assembling a coin cell, spring is first placed in the negative case. A spacer is placed on the top of the spring. Anode which is lithium metal is placed on the spacer.3 drops of electrolyte are placed on the Li metal and then place the separator. Separators are soaked in a beaker with electrolyte for about 5 min prior assembly. Electrolyte helps facilitate lithium-ion transfer between counter electrode and working electrode. Inadequate electrolyte will decrease the power the coin cell by increasing its internal resistance. If there is too much electrolyte, the electrolyte will spill out during the crimping process, but it will not harm the properties of the cell.

Place another 3 drops electrolyte on the separator, and then place the cathode. Place the positive case at last and press the cell together.

After all elements are aligned, crimp the coin cell by using a compact hydraulic crimping machine. The cell can be crimped up to a pressure of 1500 psi. After fabrication, remove the cell from the glovebox.

3.3 Formation cycling procedure

Formation cycling is the process which charge and discharge the coin cell between upper and lower voltage limits at a constant low current (C/20). The upper and lower voltage limits are determined by the electrode materials. The reason for doing formation cycle is to build up the film that forms on the surface of the electrode (called the solid-electrolyte interphase layer - SEI), which allows for a more smooth, stable flow of Li ions and prevents internal shorting. After formation, cells can undergo a suite of initial characterization tests and measurements.

When doing the formation cycling, first verify that the cell holds a voltage (the measured voltage should be >3V). If the cell doesn't hold a voltage, the cell may have shorted and cannot be used. Then the cells should be charged and discharged at a current rate of C/20 rate between upper and lower voltage (the voltage limits depend on if we are using an anode or cathode – these limits are appropriate for the $LiFePO_4$ cathodes typically on the order of 2.5 V lower to 3.6 V upper). Since the true capacity of the coin cell is not known prior to the formation cycling, the C/20 rate can be approximated by calculating a theoretical capacity according to: Q=qALρ, where q is the specific capacity of the electrode material (Ah/kg), A is the electrode

disk area (m^2), L is the electrode thickness (m), and rho is the material density (kg/m^3).

In order to charge and discharge the coin cell by using the coin cell cycler, a software program called MITS Pro is used. Figure 12 shows the main screen for the MITS Pro software interface. In order to finish once formation cycling, set 3 minutes rest at first. Then charge the cell at a constant current rate of C/20. After the charging, set 30 minutes rest, and then discharge at a constant current rate of C/20.

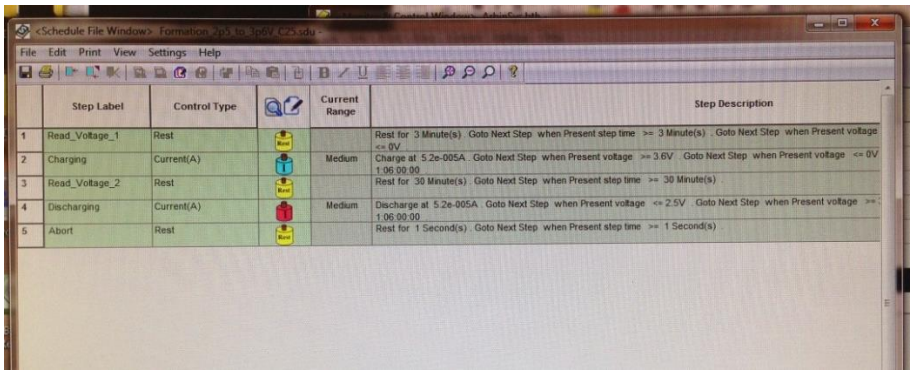

Figure 13 the setting for the formation cycling

There are some constraints need to be set when doing the charging and discharge. When the cell is being charged, the charging step could be finished and turn into next step if the voltage is charged to the high limit. If the voltage is smaller than the lower limit or the charging step time is greater than 30 hours, the charging step will be ended. The cycler records data every second. For discharging, the discharging step could turn into next step if the voltage is discharged to the low limit. And the discharging will be ended if the voltage is greater than the upper limit or the charging step time is greater than 30 hours.

In order to analyze the charging and discharging characterizations, the charging and discharging processes are repeated on 5 cells for 4 times.

Chapter 4: Results and Discussion

4.1. Description of capacity test

In order to conduct the formation cycles and evaluate the variations in the capacity and internal resistance capacity of the coin cell samples, all cells are cyclically charged and discharged at a constant low current (C/20), and between an upper and lower voltage limit. The current and voltage profiles from a sample test are represented in figure 13. When doing the test, the cell is first rested for 3 minutes, and then charged at a constant current rate to the upper voltage limit. After charging process, the input current is set to zero and the cell is held at rest conditions for 30 minutes. And then, the cell is discharged at a constant current rate to the lower voltage limit. In figure 13, I>0 means charging and I<0 means discharging.

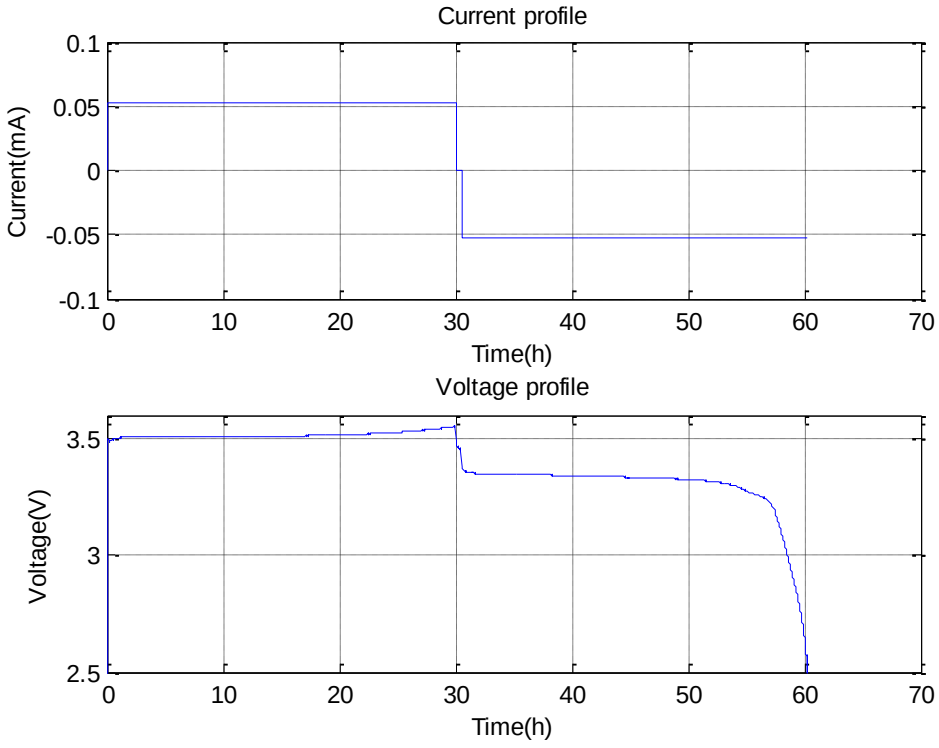

Figure 14 Current and Voltage profile during charging and discharging

In order to automate the tests, safety procedures were implemented in the Arbin cycler to stop the test in case specific events are triggered. First, each phase of the test is ended if the measured voltage reaches some pre-established limits (specifically, 3.6V during charging 2.5Vs during discharging. Furthermore, a second constraint was applied, limiting the time for which each cell is subject to the input current during the charging or the discharging phase. If the rate of current drawn is C/20, the cell should in principle require 20 hours to reach each voltage limit. In reality, this does not always occur, due to the high internal resistance and/or fabrication errors that could prevent the cell from reaching the threshold voltage. For this reason, the duration of each portion of the test (charging and discharging) is limited to 30 hours.

4.2 Result of capacity test for cell #1

Figures 14-15 show the cell voltage vs. capacity during the charging and discharging portion of the formation cycle illustrated in Figure 13. The results were obtained for the first formation cycle of cell #1.

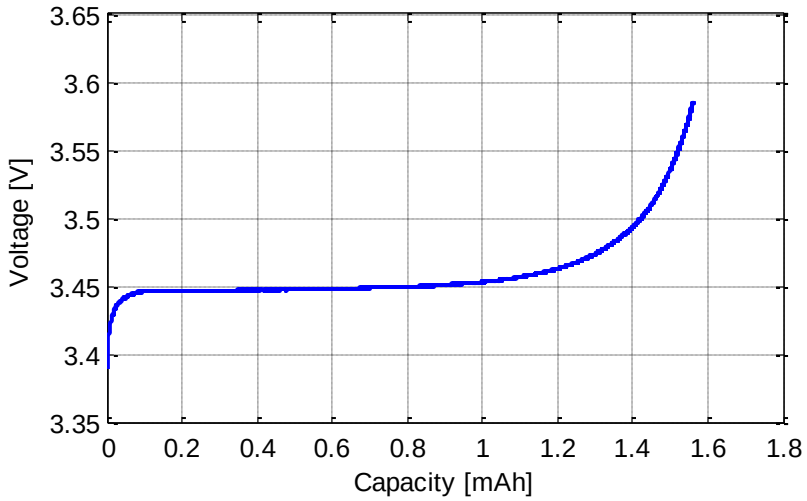

Figure 15 Charging profile for cell 1, cycle #1

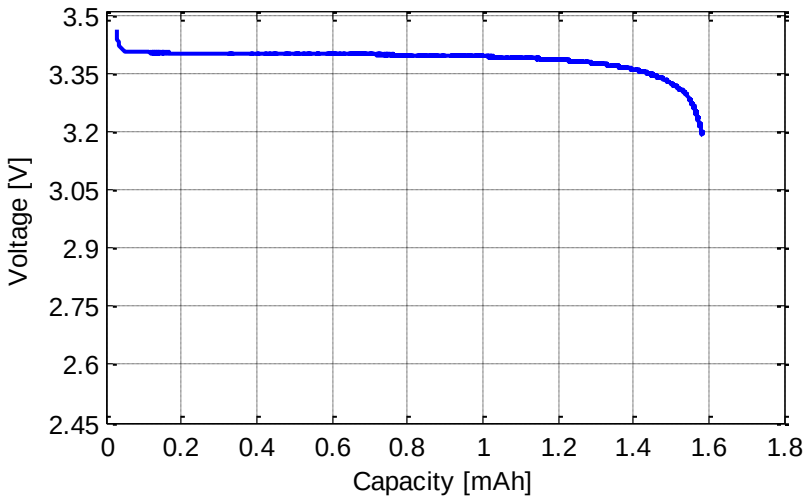

Figure 16 Discharging profile for cell 1, cycle #1

Looking at the first part of the test (Figure 14), the cell begins the charging process starting from approximately 3.4V, after a rest phase. The capacity is obtained by directly integrating the constant current over the charging portion of the test. It can be observed that the cell does not reach the upper voltage threshold (3.6V), because the maximum charge time is reached first. For this reason, the capacity (mAh) during the charging process cannot be precisely evaluated from the test data.

A similar problem occurs during the discharging portion. After the rest from the charging phase, the cell begins discharging from 3.45V, and reaches only 3.2V after 30 hours. Furthermore, interrupting each charge and discharge cycle before the threshold voltage is reached forces the cell to settle to a different relaxed voltage, hence starting the following phase (discharge or charge) from a different initial voltage condition. This means that the lithium concentration in the electrode at the beginning of each phase is different for each test, thus making it difficult to obtain an estimate of the cell capacity.

To this extent, a post-processing is done on the experimental data to approximate the value of the cell capacity. Specifically, the charging and discharging data are extrapolated to define the charge (mAh) condition at which the maximum and minimum voltage thresholds are reached. The procedure is detailed as follows:

1. A fourth-order Fourier series is used to interpolate the charge and discharge voltage data (this function has been shown to well approximate the typical OCV profile of $LiFePO_4$ electrodes):

$$V = a_0 + a_1\cos(\omega C) + b_1\sin(\omega C) + a_2\cos(\omega C) + b_2\sin(\omega C) + a_3\cos(\omega C) + b_3\sin(\omega C) + \\ + a_4\cos(\omega C) + b_4\sin(\omega C)$$

where C is the instantaneous cell charge;

2. The 10 parameters of the above fourth-order Fourier series are identified on the capacity test data using a least-square curve fitting algorithm;

3. The function is then extrapolated to find the charge value at which the voltage threshold is reached.

Figures 16-17 illustrate the results of the procedure, respectively for the charging and discharging portion of the test.

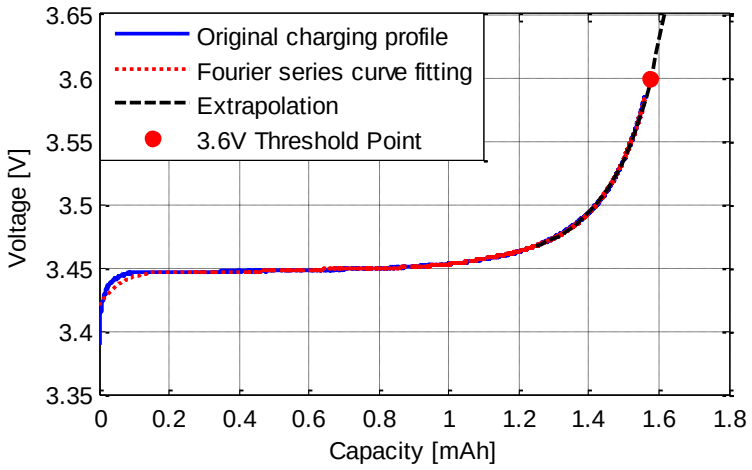

Figure 17 Extrapolated charging data for cell 1, cycle #1

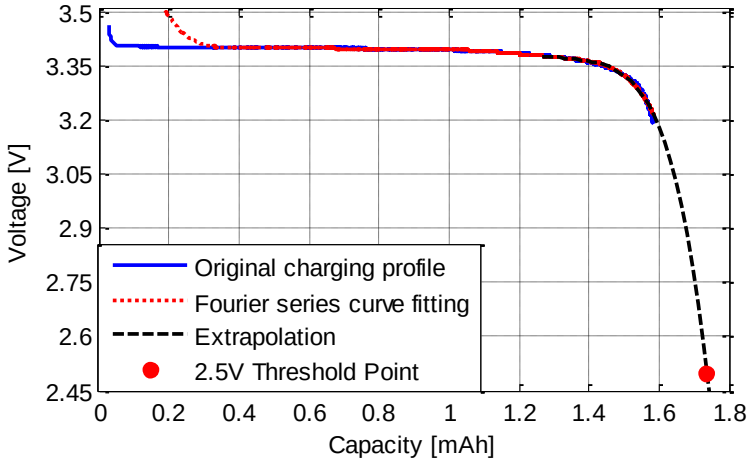

Figure 18 Extrapolated discharging data for cell 1, cycle #1

In the figures above, the blue lines show the original charging or discharging profile, whereas the red dotted lines indicate the profiles obtained by fitting the fourth-order Fourier series. To improve the accuracy of the extrapolation, the experimental data considered for the identification of the model parameters are limited to the last part of each test. The black lines represent the extrapolation using the curve fitting, while the red points indicate the condition where the thresholds at 3.6V or 2.5V are reached.

The procedure described above was applied to analyze four consecutive formation cycles, and the results are summarized in Table 1. Specifically, the initial cell voltage at the beginning of the charging and discharging phases is reported for each cycle, together with the final voltage reached in each test.

Since instrument is accurate up to 4mV, the voltage only can be recorded with 2 significant digits.

Cycle number	Charging initial voltage (V)	Charging final voltage (V)	Discharging initial voltage (V)	Discharging final voltage (V)
1	3.38	3.62	3.48	3.19
2	3.40	3.52	3.45	3.01
3	3.24	3.49	3.44	2.77
4	3.09	3.48	3.44	2.50

Table 1 Initial and final condition for charging and discharging (cell 1)

From the data in Table 1, it can be observed that there is a significant variation in the initial voltage and final voltage during each test and cycle, primarily due to the limitations in the testing procedure adopted. On the other hand, it can be observed that the discharging initial voltage remains fairly consistent across the four consecutive formation cycles.

According to the equation 1, in order to correctly compare the cell capacity across the different formation cycles, the minimum and maximum voltage threshold should be reached consistently at the end of each discharge or charge phase. While the extrapolation procedure provides a guess of the cell charge at the end of each phase, the cell voltage at the beginning of each phase is never the same, according to Table 1. This can be further evidenced by calculating the mean and standards deviation for the initial conditions of the charging and discharging phase of each cycle, as shown in Table 2.

Mean ($V_{initial}^{charge}$) (V)	Standard deviation ($V_{initial}^{charge}$)	Mean ($V_{initial}^{discharge}$) (V)	Standard deviation ($V_{initial}^{discharge}$)
3.28	0.15	3.45	0.02

Table 2 Mean and standard deviation of initial voltage condition, based on Table 1

Because the final voltage thresholds have been made consistent with the extrapolation, an estimate of the cell capacity can be obtained by selecting the initial

condition that presents the minimum standard deviation.

According to Table 2, the standard deviation for the discharging phase is much smaller than for the charging phase, meaning that after the charging process ends the cell relaxes to approximately the same voltage. This should provide a consistent initial condition for the discharge test.

To this extent, the cell capacity during the formation cycles is calculated by considering only the discharging portion of each cycle. Table 3 summarizes the capacity of Cell 1 during four consecutive formation cycles. According to equation 1:

$$C = \int_{V_{min}}^{V_{max}} I_m(t)dt \quad (I < 0 \; stands \; for \; discharge)$$

In which $I_m(t)$ is measured current. Assume that:

$$I_m(t) = I(t) + \delta I(t) \qquad (6)$$

Where $I(t)$ is the real current and $\delta I(t)$ is error from measurement. So the capacity can be written by:

$$C = \int_{V_{min}}^{V_{max}} I(t)dt + \int_{V_{min}}^{V_{max}} \delta I(t)dt \qquad (7)$$

In order to determine the cell capacity error, firstly, quantify error distribution considering portion of the test where the command constant current is -0.052mA. According to the specifications of instrument, the accuracy of low is ±10nA. The mean error of first cycle by subtracting the target current is

$$\delta I \text{ = 0.05200-0.05196 = 0.00004mA} \qquad (8)$$

The capacity error of cycle #1 is calculated by:

$$\delta C = \int_{V_{min}}^{V_{max}} \delta I(t)dt = 0.0012mAh \qquad (9)$$

The error analysis is repeated for 4 cycles.

Cycle number	Cell capacity (mAh)
1	1.7070±0.0012
2	1.6616±0.0015
3	1.6060±0.0024
4	1.5812±0.0021

Table 3 Capacity vs. cycle number for Cell 1

As expected, the cell capacity decreases rapidly during the first two cycles, to eventually settle to approximately 1.6mAh after the third cycle. This phenomenon is justified by the formation of the SEI layer during the initial lithiation, which forms a barrier to the flow of ions through the electrode, hence reducing the access to the active material.

4.3 Result of resistance calculation for cell #1

In order to calculate the cell internal resistance during the charging and discharging phase, the voltage difference and current difference during a sharp transient event need to be isolated. Based on the test profile shown in Figure 14, two specific events can be identified for calculation of the internal resistance. The first event occurs at the beginning of each test, when the cell is charged from rest conditions. The second event occurs after the cell has charged and rested for 30 minutes, and just before is discharged. Since the current profile can be approximated as a step starting from zero, the internal resistance can be simply calculated as:

$$R = \frac{\Delta V}{\Delta I} \quad (10)$$

In light of the above discussion, the initial voltage at which the resistance is calculated is generally not consistent across the different cycles, making it difficult to establish the initial value of the cell charge (or the state of charge)_before the cell is

charged or discharged. For this reason, a significant variability in the calculation of the internal resistance is to be expected.

Tables 4-5 summarize the charging resistance and discharging resistance respectively. Since the accuracy of voltage and current is ±4mV and ±10nA. The error of resistance can be calculated from Error transfer formula which is shown in equation 10:

$$\Delta N = \frac{\delta f}{\delta x_1}\Delta x_1 + \frac{\delta f}{\delta x_2}\Delta x_2 \qquad (11)$$

In which $N = f(x_1, x_2)$.

By using the error transfer formula, the resistance error can be determined by:

$$\frac{\delta R}{R} = \frac{1}{\Delta V}\delta V + \frac{1}{\Delta I}\delta I \qquad (12)$$

Where $\delta V, \delta I \; and \; \delta R$ present the accuracy of voltage, current and resistance.

Cycle #	$V_{initial}^{charge}$ (V)	$\Delta I_{charge} * 10^{-5}$ (A)	ΔV_{charge} (V)	R_{charge} (Ω)
1	3.38	5.204±0.001	0.019±0.004	365.104±76.864
2	3.40	5.201±0.001	0.008±0.004	153.817±76.908
3	3.24	5.208±0.001	0.018±0.004	345.622±76.805
4	3.09	5.208±0.001	0.019±0.004	364.823±76.805

Table 4 Charging resistance of cell #1

Cycle #	$V_{initial}^{discharge}$ (V)	$\Delta I_{discharge} * 10^{-5}$ (A)	$\Delta V_{discharge}$ (V)	$R_{discharge}$ (Ω)
1	3.48	5.195±0.001	0.005±0.004	96.246±76.997
2	3.45	5.192±0.001	0.005±0.004	96.302±77.042
3	3.44	5.193±0.001	0.005±0.004	96.283±77.026
4	3.44	5.204±0.001	0.005±0.004	96.080±76.864

Table 5 Discharging resistance of cell #1

Because of voltage accuracy of the instrument is ±4mV, only when ΔV is greater than 10mA, the ΔV can be considered reliable. However the resistance can

be calculated by equation 9 if and only if the time increment is nearly 0. In this testing, the time increment is 1 second which leads to the high uncertainty in $\Delta V\ and\ \Delta I$. So the resistance results are not reliable.

The internal resistance of the cell should change during the formation cycles as a result of many complex electrochemical phenomena, such as the SEI layer formation. The speed of these reactions, and therefore the resistive losses, depends on the concentration of reactants. So for example, at low SOC, the anode is lithium depleted, meaning that there is more resistance for the electrode to continue releasing lithium.

It can also be observed that the values of the internal resistance are different during the charging and discharging conditions. This is due to the direction of the lithium ion flux inside the electrode (lithiation and delithiation), whereby lithium ions deintercalate from $LiFePO_4$ (positive electrode) and transfer to Li (negative electrode) during charging, while the opposite process occurs during discharging. Lithium ions face a different resistive effect which caused by the conductivity of the electrolyte and the distance between the electrons during charging and discharging.

On the other hand, it is important to point out that significant variability is also introduced during the cell fabrication process, for which it is very difficult to identify the factors that could affect the internal resistance, and quantify their impact.

4.4 Results for cell 2-5

Table 6-9 summarize the initial and final conditions for charging and discharging for cell 2-5 respectively.

Cycle number	Charging initial voltage (V)	Charging final voltage (V)	Discharging initial voltage (V)	Discharging final voltage (V)
1	3.43	3.49	3.45	3.37
2	3.42	3.48	3.44	3.37
3	3.42	3.49	3.44	3.36
4	3.41	3.46	3.44	2.82

Table 6 Initial and final condition for charging and discharging (cell 2)

Cycle number	Charging initial voltage (V)	Charging final voltage (V)	Discharging initial voltage (V)	Discharging final voltage (V)
1	3.17	3.55	3.45	2.50
2	3.02	3.55	3.44	2.50
3	2.95	3.54	3.44	3.32

Table 7 Initial and final condition for charging and discharging (cell 3)

Cycle number	Charging initial voltage (V)	Charging final voltage (V)	Discharging initial voltage (V)	Discharging final voltage (V)
1	3.43	3.60	3.49	3.33
2	3.42	3.49	3.45	3.34
3	3.41	3.47	3.44	3.08
4	3.35	3.46	3.44	2.50

Table 8 Initial and final condition for charging and discharging (cell 4)

Cycle number	Charging initial voltage (V)	Charging final voltage (V)	Discharging initial voltage (V)	Discharging final voltage (V)
1	3.43	3.60	3.49	3.32
2	3.42	3.55	3.47	3.36
3	3.42	3.52	3.46	3.36

Table 9 Initial and final condition for charging and discharging (cell 5)

The cell #3 only has 3 cycles since when the cell is performing the fourth cycle, the voltage during charging condition increases much faster than other cycles. It can be concluded that the odd voltage behavior due to the cell is dying after a number of cycles. For the cell #5, the discharging has not finished in the fourth cycle so that it also only has 3 cycles.

The mean and standards deviation for the initial conditions of the charging and discharging phase of each cycle for cell 2-5 are shown in Table 10-13.

Mean ($V_{initial}^{charge}$) (V)	Standard deviation ($V_{initial}^{charge}$) (V)	Mean ($V_{initial}^{discharge}$) (V)	Standard deviation ($V_{initial}^{discharge}$) (V)
3.42	0.007	3.44	0.005

Table 10 Mean and standard deviation of initial voltage condition, based on Table 6

Mean ($V_{initial}^{charge}$) (V)	Standard deviation ($V_{initial}^{charge}$) (V)	Mean ($V_{initial}^{discharge}$) (V)	Standard deviation ($V_{initial}^{discharge}$) (V)
3.05	0.114	3.44	0.006

Table 11 Mean and standard deviation of initial voltage condition, based on Table 7

Mean ($V_{initial}^{charge}$) (V)	Standard deviation ($V_{initial}^{charge}$) (V)	Mean ($V_{initial}^{discharge}$) (V)	Standard deviation ($V_{initial}^{discharge}$) (V)
3.40	0.037	3.45	0.023

Table 12 Mean and standard deviation of initial voltage condition, based on Table 8

Mean ($V_{initial}^{charge}$) (V)	Standard deviation ($V_{initial}^{charge}$) (V)	Mean ($V_{initial}^{discharge}$) (V)	Standard deviation ($V_{initial}^{discharge}$) (V)
3.42	0.006	3.47	0.012

Table 13 Mean and standard deviation of initial voltage condition, based on Table 9

According to Table 10-13, almost for all the cells, the standard deviation for the discharging phase is smaller than for the charging phase except cell #5. However, generally, it still can be concluded the initial condition for the discharge test is more consistent than the charge test.

The capacities for cell 2-5 are shown in table 14-17.

Cycle number	Cell capacity (mAh)
1	2.0874±0.0003
2	2.1783±0.0001
3	1.9186±0.0001
4	1.6113±0.0001

Table 14 Capacity vs. cycle number for Cell 2

Cycle number	Cell capacity (mAh)
1	1.5733±0.0027
2	1.5015±0.0021
3	0.6729±0.0018

Table 15 Capacity vs. cycle number for Cell 3

Cycle number	Cell capacity (mAh)
1	1.6187±0.0033
2	1.7210±0.0033
3	1.6793±0.0030
4	1.5743±0.0027

Table 16 Capacity vs. cycle number for Cell 4

Cycle number	Cell capacity (mAh)
1	2.0467±0.0036
2	2.0040±0.0030
3	1.9379±0.0027

Table 17 Capacity vs. cycle number for Cell 5

From table 14-17, for all the cells, capacities decrease rapidly during the first two cycles, to eventually settle to approximately 1.6mAh after the third cycle except cell #3. This is because the fabrication error may occur in the cell #3 such as electrolyte deficient, which would limit the ability of lithium ions to transport, increasing the resistance. Or there may have been a problem with the crimping process and not enough pressure is being applied to the cell components. Otherwise, the electrode may have some surface impurities that are prohibiting lithium

transport. Thus, the results of cell #3 are excluded due to inconsistent data.

Tables 18-23 summarize the charging resistance and discharging resistance for cell 2-5 except cell #3.

Cycle #	$V_{initial}^{charge}$ (V)	$\Delta I_{charge} * 10^{-5}$ (A)	ΔV_{charge} (V)	R_{charge} (Ω)
1	3.43	5.211±0.001	0.015±0.004	287.853±76.761
2	3.42	5.208±0.001	0.020±0.004	384.025±76.805
3	3.42	5.208±0.001	0.025±0.004	480.031±76.805
4	3.41	5.204±0.001	0.011±0.004	211.376±76.864

Table 18 Charging resistance of cell #2

Cycle #	$V_{initial}^{discharge}$ (V)	$\Delta I_{discharge} * 10^{-5}$ (A)	$\Delta V_{discharge}$ (V)	$R_{discharge}$ (Ω)
1	3.45	5.203±0.001	0.003±0.004	57.659±76.918
2	3.44	5.196±0.001	0.006±0.004	115.473±76.982
3	3.44	5.196±0.001	0.003±0.004	57.737±76.983
4	3.44	5.200±0.001	0.003±0.004	57.692±76.923

Table 19 Discharging resistance of cell #2

Cycle #	$V_{initial}^{charge}$ (V)	$\Delta I_{charge} * 10^{-5}$ (A)	ΔV_{charge} (V)	R_{charge} (Ω)
1	3.43	5.197±0.001	0.037±0.004	711.949±76.967
2	3.42	5.193±0.001	0.028±0.004	539.187±77.027
3	3.41	5.194±0.001	0.018±0.004	346.554±77.012
4	3.35	5.190±0.001	0.018±0.004	346.821±77.071

Table 20 Charging resistance of cell #4

Cycle #	$V_{initial}^{discharge}$ (V)	$\Delta I_{discharge} * 10^{-5}$ (A)	$\Delta V_{discharge}$ (V)	$R_{discharge}$ (Ω)
1	3.49	5.185±0.001	0.008±0.004	154.291±77.146
2	3.45	5.193±0.001	0.007±0.004	134.797±77.027
3	3.44	5.194±0.001	0.005±0.004	96.265±77.012
4	3.44	5.194±0.001	0.005±0.004	96.265±77.012

Table 21 Discharging resistance of cell #4

Cycle #	$V_{initial}^{charge}$ (V)	$\Delta I_{charge} * 10^{-5}$ (A)	ΔV_{charge} (V)	R_{charge} (Ω)
1	3.43	5.205±0.001	0.022±0.004	422.671±76.849
2	3.42	5.205±0.001	0.015±0.004	288.184±76.849
3	3.42	5.203±0.001	0.012±0.004	230.636±76.879

Table 22 Charging resistance of cell #5

Cycle #	$V_{initial}^{discharge}$ (V)	$\Delta I_{discharge} * 10^{-5}$ (A)	$\Delta V_{discharge}$ (V)	$R_{discharge}$ (Ω)
1	3.49	5.185±0.001	0.008±0.004	154.291±77.146
2	3.47	5.189±0.001	0.007±0.004	134.901±77.086
3	3.46	5.189±0.001	0.005±0.004	96.358±77.086

Table 23 Discharging resistance of cell #5

From table 18-23, it can also be observed that the values of the internal resistance changes with cycling. While comparing with cell #1, almost all other cells are having a decreasing internal charging and discharging resistance with cycling except the charging resistance of cell #2 keeping a constant one. However, there are many reasons will cause the differences of internal resistance such as fabrication errors, temperature and state of capacity. It is very difficult to identify the factors that could affect the internal resistance, and quantify their impact.

4.5 Results summary for all cells

In order to conclude the charging/discharging characterization of the lithium iron phosphate material, the capacities and internal resistances of all the cells are plotted with cycling numbers. Figure 18 shows the relationship between the capacity and cycle number. Figure 19 and 20 shows the relationship between charging internal resistance/discharging internal resistance and cycle number respectively.

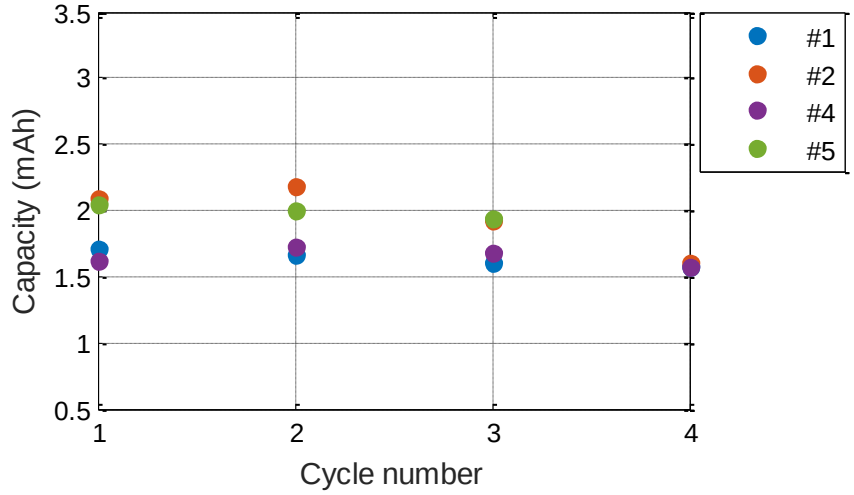

Figure 19 Capacity vs. Cycle number

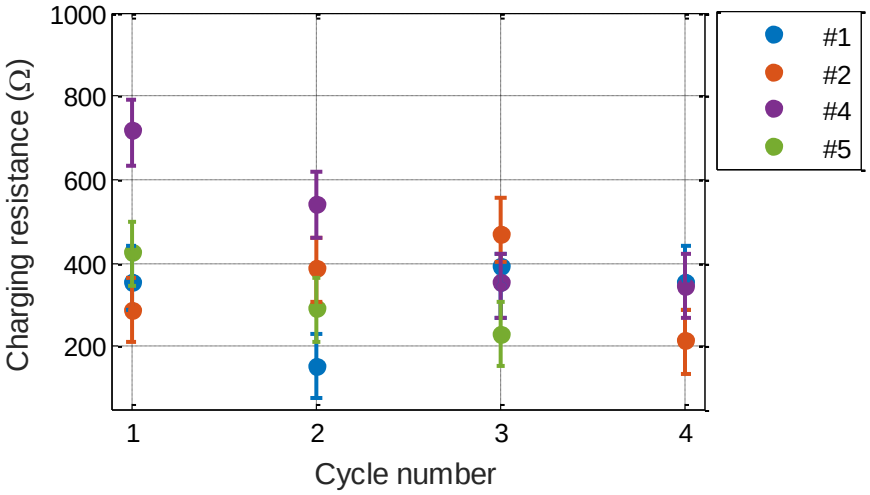

Figure 20 Charging resistance vs. Cycle number

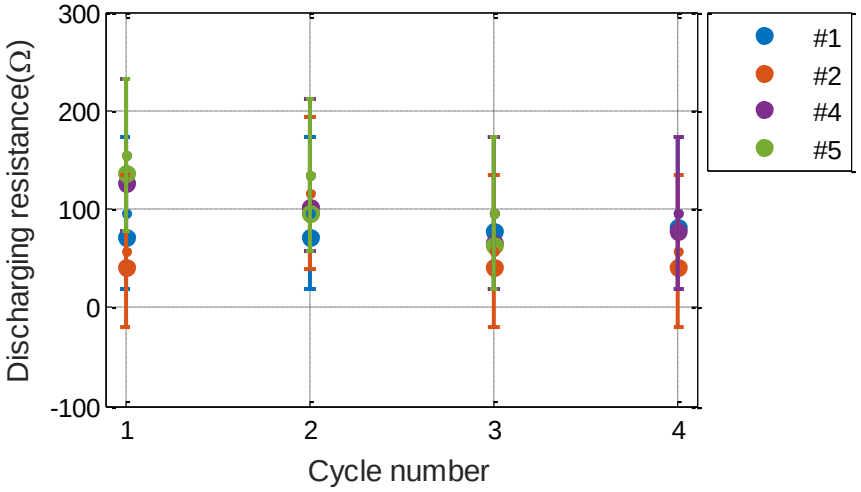

Figure 21 Discharging resistance vs. Cycle number

From figure 18, it can be observed that the cell capacity decreases with cycling. After the third cycle, the capacities of all the cells eventually settle to approximately 1.6mAh. This can be further evidenced by calculating the mean and standards deviation for the capacity of each cycle, as shown in Table 23.

(Capacity)	Cycle 1	Cycle 2	Cycle 3	Cycle 4
Mean (mAh)	1.8066	1.8133	1.7855	1.5889
Standard deviation (mAh)	0.2430	0.2731	0.1678	0.0197

Table 24 Mean and standard deviation of capacity for each cycle

The initial capacity is very different across the four samples, due to the variability caused by the fabrication process such as weight of materials, presence of contaminants, slight errors in assembly, etc. However, the cell-to-cell variation drops significantly after the third cycle. After the fourth cycle, all cells converge to the same capacity value, close to 1.6mAh.

The behavior of internal resistance cannot be concluded precisely from the figure due to there are many unknown factor will influence the internal resistance. The mean and standard deviation of the charging resistance and the discharging resistance is shown in table 25 and 26 respectively.

(Charging)	Cycle 1	Cycle2	Cycle 3	Cycle 4
Mean (Ω)	447.89	342.75	361.99	304.47
Standard deviation (Ω)	189.60	162.96	100.27	79.13

Table 25 Mean and standard deviation of charging resistance for each cycle

(Discharging)	Cycle 1	Cycle 2	Cycle 3	Cycle 4
Mean (Ω)	94.06	90.80	61.81	67.06
Standard deviation (Ω)	45.37	13.54	14.76	22.27

Table 26 Mean and standard deviation of discharging resistance for each cycle

In this case, however, there is a significant uncertainty associated to the way the resistance was measured (since the initial voltage is not always the same). Despite the issues with data acquisition and processing, it is possible to observe that the internal resistance generally decreases as the cells are progressively cycled, as expected. The standard deviation also decreases slightly during the formation cycles.

To obtain better estimate better estimates for internal resistance, more experiments could be performed. For example measuring the internal resistance with lower Δt, besides, more steps can be taken in current at different SOC.

Chapter 5: Conclusion and Future Work

In conclusion, this research investigates the influence of formation cycles on the capacity and internal resistance of Lithium-ion cells, using half-cell fabrication and testing. Experimental data were collected for several cells, subjected to four consecutive charge and discharge cycles. A fourth-order Fourier series was used to interpolate the charge and discharge voltage profile. And the function is then extrapolated to find the charge value at which the voltage threshold is reached.

Analysis and post-processing of the data allow to obtain estimates of the cell capacity and internal resistance, and observe their evolution during the formation cycles. The formation cycles contribute to “stabilize” the cell capacity and internal resistance to constant values, removing the initial variability caused by the fabrication and assembly process. The cell capacity generally decreases during the formation cycles, due to the SEI layer formation which creates a “barrier” and reduces the active sites in the electrode. On the other hand, the internal resistance generally decreases, as the morphology of the electrode and electrolyte materials changes due to the passage of current and ionic species.

Given the small number of samples, the data could not be validated with more data sets. For the future work, additional fabrication and testing of coin cells could help in confirming the initial findings. Also, more formation cycles could be completed to observe whether the capacity will remain stable.

References

[1] Simon Robinson, “The Dozen Most Important Cars of All Time-Toyota Prius (1997-present),”*Time* (2007)

[2] Richard S. Chang, “Sportier but Thirstier, a Hybrid Honda Tries to Be Hip,”*The New York Times* (2010)

[3] Bryan Walsh, “The History of the Electric Car-Green Motors,”*Time* (2007)

[4] C. Liao, H. Li, L. Wang, “A Dynamic Equivalent Circuit Model of LiFePO4 Cathode Material for Lithium Ion Batteries on Hybrid Electric Vehicles”, *Vehicle Power and Propulsion Conference* (2009)

[5] MIT Electric Vehicle Team, “A Guide to Understanding Battery Specifications” (2008).

[6] J. Belt, V. Utgikar, I. Bloom, “Calendar and PHEV cycle life aging of high-energy, lithiumion cells containing blendedspinel and layered-oxide cathodes,”*Journal of Power Sources* **196,**10213– 10221(2011).

[7] Christopher D. Rahn and Chao-Yang Wang, “Battery System Engineering,” A John Wiley & Sons, Ltd., Publication (2013).

[8] L. Faulkner, “Understanding Electrochemistry: Some Distinctive Concepts”, University of Illinois

[9] Zhang, Y. and Wang, C.Y. (2009) Cycle-life characterization of automotive lithium-ion batteries with LiNiO2 cathode. Journal of The Electrochemical Society, 156 (7), A527–A535.

[10] Battery Handbook

[11] VWR, “VWR® symphony™ Vacuum Ovens”, https://us.vwr.com/

[12] MTI Corporation, “Compact Hydraulic Crimping Machine”, http://mtixtl.com/

[13] MTI Corporation, http://mtixtl.com/